

Structural consequences of the one-electron reduction of d^4 $[\text{Mo}(\text{CO})_2(\eta\text{-PhC}\equiv\text{CPh})\text{Tp}']^+$ and the electronic structure of the d^5 radicals $[\text{M}(\text{CO})\text{L}(\eta\text{-MeC}\equiv\text{CMe})\text{Tp}']$ $\{\text{L} = \text{CO}$ and $\text{P}(\text{OCH}_2)_3\text{CEt}\}^\ddagger$

Christopher J. Adams,^a Ian M. Bartlett,^a Supakorn Boonyuen,^a Neil G. Connelly,^{*a} David J. Harding,^a Owen D. Hayward,^a Eric J. L. McInnes,^b A. Guy Orpen,^a Michael J. Quayle^a and Philip H. Rieger^{‡c}

Received 24th October 2005, Accepted 8th February 2006

First published as an Advance Article on the web 2nd March 2006

DOI: 10.1039/b514951g

Reduction of $[\text{M}(\text{CO})_2(\eta\text{-RC}\equiv\text{CR}')\text{Tp}']\text{X}$ $\{\text{Tp}' = \text{hydrotris}(3,5\text{-dimethylpyrazolyl})\text{borate}$, $\text{M} = \text{Mo}$, $\text{X} = [\text{PF}_6]^-$, $\text{R} = \text{R}' = \text{Ph}$, $\text{C}_6\text{H}_4\text{OMe-4}$ or Me ; $\text{R} = \text{Ph}$, $\text{R}' = \text{H}$; $\text{M} = \text{W}$, $\text{X} = [\text{BF}_4]^-$, $\text{R} = \text{R}' = \text{Ph}$ or Me ; $\text{R} = \text{Ph}$, $\text{R}' = \text{H}\}$ with $[\text{Co}(\eta\text{-C}_5\text{H}_5)_2]$ gave paramagnetic $[\text{M}(\text{CO})_2(\eta\text{-RC}\equiv\text{CR}')\text{Tp}']$, characterised by IR and ESR spectroscopy. X-Ray structural studies on the redox pair $[\text{Mo}(\text{CO})_2(\eta\text{-PhC}\equiv\text{CPh})\text{Tp}']$ and $[\text{Mo}(\text{CO})_2(\eta\text{-PhC}\equiv\text{CPh})\text{Tp}'][\text{PF}_6]$ showed that oxidation is accompanied by a lengthening of the $\text{C}\equiv\text{C}$ bond and shortening of the $\text{Mo}\text{-C}_{\text{alkyne}}$ bonds, consistent with removal of an electron from an orbital antibonding with respect to the $\text{Mo}\text{-alkyne}$ bond, and with conversion of the alkyne from a three- to a four-electron donor. Reduction of $[\text{Mo}(\text{CO})(\text{NCMe})(\eta\text{-MeC}\equiv\text{CMe})\text{Tp}'][\text{PF}_6]$ with $[\text{Co}(\eta\text{-C}_5\text{H}_5)_2]$ in CH_2Cl_2 gives $[\text{MoCl}(\text{CO})(\eta\text{-MeC}\equiv\text{CMe})\text{Tp}']$, via nitrile substitution in $[\text{Mo}(\text{CO})(\text{NCMe})(\eta\text{-MeC}\equiv\text{CMe})\text{Tp}']$, whereas a similar reaction with $[\text{M}(\text{CO})\{\text{P}(\text{OCH}_2)_3\text{CEt}\}(\eta\text{-MeC}\equiv\text{CMe})\text{Tp}']^+$ ($\text{M} = \text{Mo}$ or W) gives the phosphite-containing radicals $[\text{M}(\text{CO})\{\text{P}(\text{OCH}_2)_3\text{CEt}\}(\eta\text{-MeC}\equiv\text{CMe})\text{Tp}']$. ESR spectroscopic studies and DFT calculations on $[\text{M}(\text{CO})\text{L}(\eta\text{-MeC}\equiv\text{CMe})\text{Tp}']$ $\{\text{M} = \text{Mo}$ or W , $\text{L} = \text{CO}$ or $\text{P}(\text{OCH}_2)_3\text{CEt}\}$ show the SOMO of the neutral d^5 species (the LUMO of the d^4 cations) to be largely d_{yz} in character although much more delocalised in the W complexes. Non-coincidence effects between the g and metal hyperfine matrices in the Mo spectra indicate hybridisation of the metal d -orbitals in the SOMO, consistent with a rotation of the coordinated alkyne about the $\text{M}\text{-C}_2$ axis.

Introduction

During our studies of the redox properties of metal–alkyne complexes¹ we have shown that oxidation of the (formal) d^6 complex $[\text{Cr}(\text{CO})_2(\eta\text{-PhC}\equiv\text{CPh})(\eta\text{-C}_6\text{Me}_5\text{H})]$ to the d^5 cation $[\text{Cr}(\text{CO})_2(\eta\text{-PhC}\equiv\text{CPh})(\eta\text{-C}_6\text{Me}_5\text{H})]^+$ results in a shortening of the $\text{Cr}\text{-C}_{\text{alkyne}}$ bonds, in accord with electron loss from a HOMO antibonding with respect to the metal–alkyne bond and with the conversion of the alkyne from a two- to a three-electron donor.² Preliminary studies showed³ that oxidation of d^5 $[\text{Mo}(\text{CO})_2(\eta\text{-PhC}\equiv\text{CPh})\text{Tp}']$ to d^4 $[\text{Mo}(\text{CO})_2(\eta\text{-PhC}\equiv\text{CPh})\text{Tp}']^+$ $\{\text{Tp}' = \text{hydrotris}(3,5\text{-dimethylpyrazolyl})\text{borate}\}$ resulted in a similar shortening of the $\text{Mo}\text{-C}_{\text{alkyne}}$ bonds as the alkyne was converted from a three-electron to a four-electron donor. We now give details of these structural changes, of the reduction of $[\text{M}(\text{CO})\text{L}(\eta\text{-RC}\equiv\text{CR}')\text{Tp}']^+$ $\{\text{M} = \text{Mo}$ or W , $\text{L} = \text{CO}$ or $\text{P}(\text{OCH}_2)_3\text{CEt}\}$ to $[\text{M}(\text{CO})\text{L}(\eta\text{-RC}\equiv\text{CR}')\text{Tp}']$ $\{\text{L} = \text{CO}$ or $\text{P}(\text{OCH}_2)_3\text{CEt}\}$, and of ESR spectroscopic studies and DFT calculations which provide

further insight into the electronic structure of the paramagnetic complexes.

Results and discussion

The synthesis and reduction of $[\text{M}(\text{CO})_2(\eta\text{-RC}\equiv\text{CR}')\text{Tp}']^z$ ($z = 0$ and 1)

In order to study their redox properties, the known complexes $[\text{W}(\text{CO})_2(\eta\text{-RC}\equiv\text{CR}')\text{Tp}'][\text{BF}_4]$ ($\text{R} = \text{R}' = \text{Ph}$ or Me ; $\text{R} = \text{Ph}$, $\text{R}' = \text{H}$) were prepared by the published method⁴ and the new analogues $[\text{Mo}(\text{CO})_2(\eta\text{-RC}\equiv\text{CR}')\text{Tp}'][\text{PF}_6]$ ($\text{R} = \text{R}' = \text{Ph}$, 1^+ ; $\text{C}_6\text{H}_4\text{OMe-4}$, 2^+ or Me , 3^+ ; $\text{R} = \text{Ph}$, $\text{R}' = \text{H}$, 4^+) by the oxidation of $[\text{Mo}(\text{CO})_3\text{Tp}']$ with $[\text{Fe}(\eta\text{-C}_5\text{H}_5)_2][\text{PF}_6]$ in the presence of the alkyne. The new complexes were characterised by elemental analysis and IR (Table 1) and NMR spectroscopy, with assignments of the latter spectra made on the basis of those for $[\text{W}(\text{CO})_2(\eta\text{-RC}\equiv\text{CR}')\text{Tp}'][\text{BF}_4]$.⁴ The ^1H NMR spectra of the $4\text{-MeOC}_6\text{H}_4\text{C}\equiv\text{CC}_6\text{H}_4\text{OMe-4}$ and $\text{MeC}\equiv\text{CMe}$ complexes 2^+ and 3^+ each showed two methyl resonances for the alkyne substituents, and the ^{13}C spectra of the complexes of symmetrical alkynes (*i.e.* $\text{R} = \text{R}'$) each showed two peaks for the coordinated carbons (with chemical shifts in the region associated with four-electron alkyne ligands^{5,6}). Thus, there is little or no alkyne rotation at room temperature.

Cyclic voltammetry shows that the new cationic dicarbonyls 1^+ – 4^+ and $[\text{W}(\text{CO})_2(\eta\text{-RC}\equiv\text{CR}')\text{Tp}'][\text{BF}_4]$ ($\text{R} = \text{R}' = \text{Ph}$, 5^+ or Me , 6^+ ;

^aSchool of Chemistry, University of Bristol, Bristol, BS8 1TS, UK. E-mail: neil.connelly@bristol.ac.uk; Fax: +44 (0)117 929 0509; Tel: +44 (0)117 928 8162

^bSchool of Chemistry, University of Manchester, Manchester, M13 9PL, UK

^cDepartment of Chemistry, Brown University, Rhode Island, RI 02912, USA

† Electronic supplementary information (ESI) available: ^1H , $^{13}\text{C}\{^1\text{H}\}$ and ^{31}P NMR spectroscopic data for the alkyne complexes. See DOI: 10.1039/b514951g

‡ Deceased.

Table 1 Analytical, IR spectroscopic and electrochemical data for alkyne complexes

| Complex | Colour | Yield (%) | Analysis (%) ^a | | | | IR ^b /cm ⁻¹ ν(CO) | E ^o , b, c /V |
|---|--------------|-----------|---------------------------|-----------|------------|------------|---|--------------------------|
| | | | C | H | N | | | |
| [Mo(CO) ₂ (η-PhC≡CPh)Tp][PF ₆] ⁺ 1 ⁺ [PF ₆] ⁻ | Crimson-red | 60 | 44.9 (44.8) ^d | 4.0 (4.0) | 9.7(9.8) | 2065, 2003 | -0.10 (-1.33 ^e) | |
| [Mo(CO) ₂ (η-R'C≡CR)Tp][PF ₆] ²⁺ 2 ⁺ [PF ₆] ⁻ (R = C ₆ H ₄ OMe-4) | Crimson-red | 65 | 46.2 (46.3) ^f | 3.8 (3.6) | 9.8(9.7) | 2054, 1989 | -0.24 (-1.39 ^e) [1.55] | |
| [Mo(CO) ₂ (η-MeC≡CMe)Tp][PF ₆] ³⁺ 3 ⁺ [PF ₆] ⁻ | Green | 60 | 38.9 (38.9) | 4.5 (4.3) | 13.1(13.0) | 2066, 1997 | -0.18 | |
| [Mo(CO) ₂ (η-PhC≡CH)Tp][PF ₆] ⁴⁺ 4 ⁺ [PF ₆] ⁻ | Orange-brown | 48 | 39.9 (40.0) ^d | 3.9 (3.9) | 10.7(10.8) | 2074, 2010 | -0.05 (-1.28 ^e) | |
| [W(CO) ₂ (η-PhC≡CPh)Tp][BF ₄] ⁵⁺ 5 ⁺ [BF ₄] ⁻ | Green | | | | | 2053, 1980 | -0.40 (-1.45) | |
| [W(CO) ₂ (η-MeC≡CMe)Tp][BF ₄] ⁶⁺ 6 ⁺ [BF ₄] ⁻ | Blue-green | | | | | 2055, 1975 | -0.49 (-1.58) | |
| [W(CO) ₂ (η-PhC≡CH)Tp][BF ₄] ⁷⁺ 7 ⁺ [BF ₄] ⁻ | Green | | | | | 2062, 1987 | -0.34 (-1.40) | |
| [Mo(CO)(NCMe)(η-MeC≡CMe)Tp][PF ₆] ⁸⁺ 8 ⁺ [PF ₆] ⁻ | Pale green | 76 | 42.6 (42.6) ^d | 5.6 (5.4) | 13.2(13.4) | 1959 | -0.95 ^f [1.17] | |
| [W(CO)(P(OCH ₃) ₂ CEt)(η-MeC≡CMe)Tp][BF ₄] ¹⁰⁺ 10 ⁺ [BF ₄] ⁻ | Blue | 26 | 35.9 (36.2) ^d | 4.6 (4.6) | 9.2(9.4) | 1965 | -1.01 [1.28] | |
| [Mo(CO){P(OCH ₃) ₂ CEt}(η-MeC≡CMe)Tp][PF ₆] ¹¹⁺ 11 ⁺ [PF ₆] ⁻ | Green | 47 | 38.4 (38.6) ^f | 5.1 (4.9) | 9.9(10.2) | 1984 | -0.66 [1.39] | |

^a Calculated values in parentheses. ^b In CH₂Cl₂. ^c Potential for the reversible, diffusion-controlled, one-electron reduction to [M(CO)L(η-R'C≡CR')Tp]⁻. Where applicable, the potential for the second reduction process is shown in parentheses and that for the reversible one-electron oxidation in square brackets. ^d Analysed as a 1.0 CH₂Cl₂ solvate. ^e The potential of the second reduction wave is fully reversible in the presence of [Co(η-C₅H₅)₂][BF₄] as internal calibrant. In the absence of the calibrant the wave is less well defined (see text). ^f Analysed as a 0.5 CH₂Cl₂ solvate. ^g Compound reported in ref. 4. ^h Analysed as a 1.0 thf solvate. ⁱ Irreversible reduction wave with associated reversible product wave centred at 0.61 V.

R = Ph, R' = H, 7⁺) undergo reversible one-electron reduction in the potential range 0.0 to -0.5 V (Table 1), with the potential depending on the alkyne (E^o = 4-MeOC₆H₄C≡CC₆H₄OMe-4 < MeC≡CMe < PhC≡CPh < PhC≡CH) and the metal; the tungsten complexes are more difficult to reduce than the molybdenum analogues by ca. 300 mV. Most complexes also show a second reduction wave at a potential more negative than the first by ca. -1.1 to -1.2 V. Interestingly, the reversibility of the second wave is enhanced in the presence of [Co(η-C₅H₅)₂][BF₄] (added to the electrochemical cell as an internal standard of potential, reduction potential -0.86 V) suggesting some mediation of heterogeneous electron transfer to the platinum electrode. This second reduction would correspond to the formation of the d⁶ anion [Mo(CO)₂(η-R'C≡CR')Tp]⁻, isoelectronic with [Cr(CO)₂(η-R'C≡CR')(arene)]²⁻.

On the basis of the potentials measured for the first reduction process, treatment of [Mo(CO)₂(η-R'C≡CR')Tp][PF₆]⁺ or [W(CO)₂(η-R'C≡CR')Tp][BF₄]⁺ with the one-electron reductant [Co(η-C₅H₅)₂] gave the air-sensitive neutral complexes [M(CO)₂(η-R'C≡CR')Tp]. In the case of [Mo(CO)₂(η-PhC≡CPh)Tp] **1**, the only isolable compound in this series, green-black crystals were formed after reducing [Mo(CO)₂(η-PhC≡CPh)Tp][PF₆]⁺1⁺[PF₆]⁻ in CH₂Cl₂, evaporating the dark green solution to dryness, extracting the black residue into hot *n*-hexane, and cooling the extract to -20 °C.

The paramagnetic complex **1** was characterised by elemental analysis (as a 0.5 *n*-hexane solvate—confirmed by the X-ray structural analysis, see below) and by IR spectroscopy (Table 2) which showed carbonyl bands at 1962 and 1876 cm⁻¹ in CH₂Cl₂, shifted to lower wavenumber by ca. 100–130 cm⁻¹ from the values for [Mo(CO)₂(η-PhC≡CPh)Tp][PF₆]⁺1⁺[PF₆]⁻ (2065 and 2003 cm⁻¹). The CV of the neutral complex **1** showed one oxidation wave and one reduction wave at potentials effectively identical to those for the two sequential reductions of [Mo(CO)₂(η-PhC≡CPh)Tp][PF₆]⁺1⁺[PF₆]⁻.

The analogous compounds [M(CO)₂(η-R'C≡CR')Tp] (M = Mo; R = R' = C₆H₄OMe-4 **2**, Me **3**, R = Ph, R' = H **4**; M = W; R = R' = Ph **5** or Me **6**, R = Ph, R' = H **7**) were characterised in solution, by IR (Table 2) and ESR spectroscopy, after generation by [Co(η-C₅H₅)₂] reduction of the corresponding cations *in situ*. As for **1**, the IR spectra showed two carbonyl bands shifted to lower wavenumber on reduction. The ESR spectra, together with those of the other paramagnetic species in this paper, are described below.

Complex [Mo(CO)₂(η-PhC≡CPh)Tp] **1** was also structurally characterised, enabling a comparison to be made of the redox pair [Mo(CO)₂(η-PhC≡CPh)Tp]^z (z = 0 and +1).

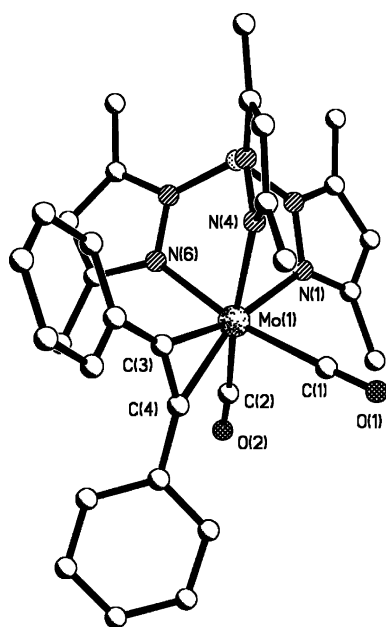
The X-ray structures of [Mo(CO)₂(η-PhC≡CPh)Tp]·0.5C₆H₁₄, 1·0.5C₆H₁₄ and [Mo(CO)₂(η-PhC≡CPh)Tp][PF₆]⁺1⁺[PF₆]⁻

The structures of [Mo(CO)₂(η-PhC≡CPh)Tp] **1** and [Mo(CO)₂(η-PhC≡CPh)Tp]⁺1⁺, previously reported in ref. 3, are generally similar; that of **1**⁺ is shown in Fig. 1 as a representative example, and selected bond lengths and angles for both **1** and **1**⁺ are given in Table 3. In both complexes, the molybdenum atom adopts a pseudo-octahedral geometry with three *fac* sites occupied by the κ³-Tp' group and two *cis* sites by the carbonyl ligands; the diphenylacetylene completes the coordination sphere.

Table 2 IR and ESR spectroscopic data for $[\text{M}(\text{CO})_2(\eta\text{-RC}\equiv\text{CR}')\text{Tp}]$ (**1–7**) and $[\text{M}(\text{CO})\{\text{P}(\text{OCH}_2)_3\text{CEt}\}(\eta\text{-RC}\equiv\text{CR}')\text{Tp}]$ (**10** and **11**)

| Complex | IR ^a /cm ⁻¹ $\nu(\text{CO})$ | M | R | R' | ESR isotropic parameters ^b | | ESR anisotropic parameters ^b | | | |
|-----------------------|--|----|-------------------------------------|-------------------------------------|---------------------------------------|--|---|------------|------------|------------------|
| | | | | | $\langle g_{\text{iso}} \rangle$ | $\langle A_{\text{iso}} \rangle / G^c$ | g_1 | g_2 | g_3 | g_{ave} |
| 1 ^c | 1962, 1876 1968, 1887 ^d | Mo | Ph | Ph | 2.007 | 30.7 | 2.036 | 2.009 | 1.977 | 2.007 |
| 2 | 1956, 1870 1963, 1881 ^d | Mo | C ₆ H ₄ OMe-4 | C ₆ H ₄ OMe-4 | 2.007 | 30.1 | 2.039 ^e | 2.009 | 1.979 | 2.009 |
| 3 | 1945, 1849 1952, 1864 ^d | Mo | Me | Me | 2.011 | 31.1 | 2.039 | 2.016 | 1.979 | 2.011 |
| 4 | 1964, 1880 1969, 1890 ^d | Mo | Ph | H | 2.008 ^f | 31.2 | 2.038 | 2.010 | 1.975 | 2.008 |
| 5 | 1948, 1854 1957, 1866 ^d | W | Ph | Ph | 2.013 | ^g | 2.098 | 2.004 | 1.947 | 2.016 |
| 6 | 1932, 1840 1941, 1856 ^d | W | Me | Me | 2.021 | 42 | 2.102 | 2.015 | 1.955 | 2.024 |
| 7 | 1950, 1857 1957, 1870 ^d | W | Ph | H | 2.016 | 50 | 2.100 | 2.006 | 1.947 | 2.018 |
| 10 | — | W | Me | Me | 2.015 ^f | ^g (19) | 2.126 ^{h,i} (11) | 2.002 (11) | 1.951 (11) | 2.026(11) |
| 11 | — | Mo | Me | Me | 2.001 ^f | 35 (32) | 2.027 ^{j,k} (32) | 1.990 (37) | 1.944 (36) | 1.987 (35) |

^a In CH₂Cl₂ unless otherwise stated. ^b In toluene at 290–300 K (isotropic) or 77 K (anisotropic) unless stated otherwise. ^c Metal hyperfine coupling; ³¹P coupling in parentheses. ^d In *n*-hexane. ^e At 110 K. ^f At 240 K in CH₂Cl₂ : thf (1 : 2). ^g Not resolved. ^h At 110 K in CH₂Cl₂ : thf (1 : 2). ⁱ ³¹P coupling in parentheses. ^j At 120 K in CH₂Cl₂ : thf (1 : 2).

**Fig. 1** The molecular structure of the cation $[\text{Mo}(\text{CO})_2(\eta\text{-PhC}\equiv\text{CPh})\text{Tp}]^+ \mathbf{1}^+$. Hydrogen atoms have been omitted for clarity.

The most significant structural change on reduction is the lengthening of the mean Mo–C_{alkyne} distance from 2.055 Å in **1**⁺ to 2.155 Å in **1**. Such a lengthening, also observed when the d⁵ complex $[\text{Cr}(\text{CO})_2(\eta\text{-PhC}\equiv\text{CPh})(\eta\text{-C}_6\text{Me}_5\text{H})]^+$ is reduced to d⁶ $[\text{Cr}(\text{CO})_2(\eta\text{-PhC}\equiv\text{CPh})(\eta\text{-C}_6\text{Me}_5\text{H})]^+$,² results from population of the LUMO of **1**⁺ [Fig. 2(a)] which is anti-bonding with respect to the metal–alkyne bond. {This orbital is also bonding with respect to the alkyne C–C bond so that C(3)–C(4) decreases from 1.334(6) Å in **1**⁺ to 1.282(3) Å in **1**.} Effectively, the alkyne changes from a four- to a three-electron donor as **1**⁺ is reduced to **1**. (The mean Mo–C_{alkyne} distance for **1**⁺ is in the typical range—2.06 to 2.00 Å—for four-electron molybdenum or tungsten alkyne complexes.⁶)

Table 3 Selected bond lengths (Å) and angles (°) for $[\text{Mo}(\text{CO})_2(\eta\text{-PhC}\equiv\text{CPh})\text{Tp}][\text{PF}_6] \mathbf{1}^+ [\text{PF}_6]^-$ and $[\text{Mo}(\text{CO})_2(\eta\text{-PhC}\equiv\text{CPh})\text{Tp}] \mathbf{1}^+$

| | 1 ⁺ [PF ₆] ⁻ | 1 |
|------------------------|---|-----------------------|
| Mo(1)–N _{ave} | 2.207(3) | 2.245(3) |
| Mo(1)–C(3) | 2.041(4) | 2.136(3) |
| Mo(1)–C(4) | 2.069(3) | 2.175(3) |
| C(3)–C(4) | 1.334(6) | 1.282(3) |
| Mo(1)–C(1) | 2.108(4) | 2.000(3) |
| Mo(1)–C(2) | 2.029(4) | 1.974(3) |
| C(1)–O(1) | 1.114(5) | 1.149(3) |
| C(2)–O(2) | 1.125(5) | 1.154(3) |
| C(4)–C(3)–C(14) | 141.3(3) | 140.7(2) ^b |
| C(3)–C(4)–C(5) | 142.6(3) | 143.7(2) |
| C(1)–Mo(1)–C(2) | 91.8(2) | 88.7(1) |
| β^c | 22.8, 72.4 | 22.7, 68.0 |

^a Numbering as in Fig. 1. ^b Atom numbering for this angle in **1** is C(4)–C(3)–C(15). ^c β = the angles between the C≡C and M–C(O) vectors. {The two angles relate to the two CO groups of the Mo(CO)₂ unit.}

The orientation of the alkyne, between the two Mo(CO) groups in both **1**⁺ and **1**, does not change on reduction but is very different from that in $[\text{Cr}(\text{CO})_2(\eta\text{-PhC}\equiv\text{CPh})(\eta\text{-C}_6\text{Me}_5\text{H})]^+$ ($z = 0$, d⁶ and **1**, d⁵) where the alkyne lies approximately parallel to the plane of the arene ring.² In both **1**⁺ and **1** the alkyne aligns more with one carbonyl ligand than the other of the Mo(CO)₂ group, with the angle between the C≡C and M–C(O) vector, β , ca. 23° in both cases. (Note that the observation of a 2 : 1 ratio of pyrazolyl rings in the NMR spectra of **1**⁺ suggests a facile fluxional process by which the two carbonyl ligands also become equivalent in solution, presumably alkyne oscillation but not rotation—see above.) This angle is somewhat smaller than that in $[\text{W}(\text{CO})_2(\eta\text{-PhC}\equiv\text{CMe})\text{Tp}]^+$ ($\beta = 34.5^\circ$).⁷

The preferential alignment of the alkyne with one carbonyl more than the other can be understood in terms of the nature of the HOMO of **1**⁺ [Fig. 2(b)], which also leads to the bond Mo(1)–C(2) being shorter than Mo(1)–C(1) in both **1**⁺ and **1** {1.974(3) cf. 2.000(3) in **1** and 2.029(4) cf. 2.108(4) in **1**⁺} via “a constructive

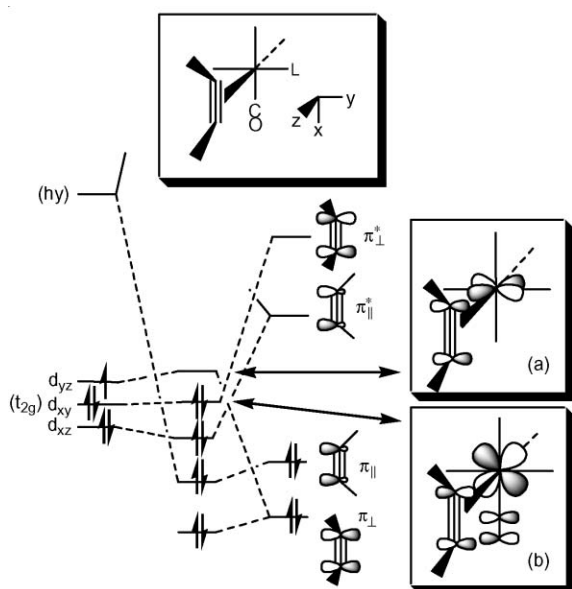


Fig. 2 Schematic MO diagram for the pseudo-octahedral complexes $[\text{Mo}(\text{CO})\text{L}(\eta\text{-alkyne})\text{Tp}]^+$. The three *fac* sites are shown as vacant. Orbital (a) is the SOMO for the d^5 species ($z = 0$) and the LUMO for the d^4 complexes ($z = 1$); orbital (b) is the HOMO for $z = 1$. (Adapted from Fig. 3 in ref. 2.)

interaction between the carbonyl carbon and the proximal alkyne carbon⁴⁴ {leading to $\text{C}(2)\text{-C}(4) = 2.482(4) \text{ \AA}$ for **1** and $2.462(6) \text{ \AA}$ **1**⁺}.

The synthesis and electrochemistry of $[\text{M}(\text{CO})(\text{NCMe})(\eta\text{-MeC}\equiv\text{CMe})\text{Tp}]^+$

The tungsten complexes $[\text{W}(\text{CO})(\text{NCMe})(\eta\text{-RC}\equiv\text{CR})\text{Tp}][\text{BF}_4]$ ($\text{R} = \text{R}' = \text{Ph}$ or Me ; $\text{R} = \text{Ph}$, $\text{R}' = \text{H}$ or Me) have been prepared previously,⁴ either by halide abstraction from $[\text{W}(\text{I})(\text{CO})(\eta\text{-RC}\equiv\text{CR})\text{Tp}]$ with $\text{Ag}[\text{BF}_4]$ in MeCN or by nitrile substitution of one CO ligand of $[\text{W}(\text{CO})_2(\eta\text{-RC}\equiv\text{CR})\text{Tp}][\text{BF}_4]$. The new molybdenum analogue $[\text{Mo}(\text{CO})(\text{NCMe})(\eta\text{-MeC}\equiv\text{CMe})\text{Tp}][\text{PF}_6]$ **8**⁺ $[\text{PF}_6]^-$ was prepared by the latter route, *i.e.* by stirring $[\text{Mo}(\text{CO})_2(\eta\text{-MeC}\equiv\text{CMe})\text{Tp}][\text{PF}_6]$ in MeCN for *ca.* 5 min. Purification using thf-*n*-hexane then gave the product as a moderately air-sensitive, pale green 1 : 1 thf solvate which was characterised by IR (Table 1) and NMR spectroscopy and cyclic voltammetry.

The presence of an asymmetric metal centre in $[\text{Mo}(\text{CO})(\text{NCMe})(\eta\text{-MeC}\equiv\text{CMe})\text{Tp}]^+$ is reflected in the ¹H and ¹³C NMR spectra which are very similar to those of $[\text{W}(\text{CO})(\text{NCMe})(\eta\text{-MeC}\equiv\text{CMe})\text{Tp}][\text{BF}_4]$ **9**⁺ $[\text{BF}_4]^-$,⁴ *i.e.* all three pyrazolyl rings of the Tp' ligand are inequivalent. Two sharp ¹H singlets, at 2.78 and 3.62 ppm, for the alkyne methyl protons, and two ¹³C resonances for the alkyne methyl substituents (21.6 and 23.5 ppm) and metal-bound carbon atoms (218.9 and 231.4 ppm) are consistent with no alkyne rotation at room temperature, and with the alkyne acting as a four-electron donor.⁶

The CV of $[\text{Mo}(\text{CO})(\text{NCMe})(\eta\text{-MeC}\equiv\text{CMe})\text{Tp}][\text{PF}_6]$ **8**⁺ $[\text{PF}_6]^-$ in CH_2Cl_2 is different from that of $[\text{Mo}(\text{CO})_2(\eta\text{-MeC}\equiv\text{CMe})\text{Tp}][\text{PF}_6]$ **3**⁺ $[\text{PF}_6]^-$ in showing a reversible oxidation wave at 1.17 V, and an irreversible reduction wave at -0.95 V associated with a reversible product wave at 0.61 V. Thus, substitution of one CO of **3**⁺ by the better donor MeCN, to give **8**⁺, results in a shift to

more negative potentials of about 0.8 V for the reduction wave. (Assuming a similar shift for the oxidation wave, the potential for the oxidation of $[\text{Mo}(\text{CO})_2(\eta\text{-MeC}\equiv\text{CMe})\text{Tp}][\text{PF}_6]$ **3**⁺ $[\text{PF}_6]^-$ would be approximately 1.9 V, outside the accessible potential range in CH_2Cl_2 .) The irreversibility of the reduction wave for **8**⁺ indicates that electron addition is followed by a rapid chemical reaction, possibly loss of MeCN.

Chemical reduction of $[\text{Mo}(\text{CO})(\text{NCMe})(\eta\text{-MeC}\equiv\text{CMe})\text{Tp}][\text{PF}_6]$ **8**⁺ $[\text{PF}_6]^-$ with $[\text{Co}(\eta\text{-C}_5\text{H}_5)_2]$ in CH_2Cl_2 resulted in the formation of a complex showing one IR carbonyl band at 1922 cm^{-1} , subsequently isolated and characterised as $[\text{MoCl}(\text{CO})(\eta\text{-MeC}\equiv\text{CMe})\text{Tp}]$.⁸ The chloro complex shows a one-electron oxidation wave at 0.61 V, identical to the product wave observed in the CV of **8**⁺. Hence, even on the timescale of cyclic voltammetry, $[\text{MoCl}(\text{CO})(\eta\text{-MeC}\equiv\text{CMe})\text{Tp}]$ is formed from $[\text{Mo}(\text{CO})(\text{NCMe})(\eta\text{-MeC}\equiv\text{CMe})\text{Tp}]^+$ presumably *via* the neutral complex $[\text{Mo}(\text{CO})(\text{NCMe})(\eta\text{-MeC}\equiv\text{CMe})\text{Tp}]$ (although this paramagnetic species has not been detected spectroscopically, *cf.* the much more stable dicarbonyl analogues **1-7**).

The synthesis and electrochemistry of $[\text{M}(\text{CO})\{\text{P}(\text{OCH}_2)_3\text{CEt}\}(\eta\text{-MeC}\equiv\text{CMe})\text{Tp}]^+$

In order to assess further the effects of L on the redox properties of $[\text{M}(\text{CO})\text{L}(\eta\text{-RC}\equiv\text{CR})\text{Tp}]^+$ (*cf.* L = CO and MeCN above) the phosphite derivatives $[\text{M}(\text{CO})\{\text{P}(\text{OCH}_2)_3\text{CEt}\}(\eta\text{-MeC}\equiv\text{CMe})\text{Tp}][\text{X}]$ ($\text{M} = \text{W}$, $\text{X} = [\text{BF}_4]^-$; $\text{M} = \text{Mo}$, $\text{X} = [\text{PF}_6]^-$) have also been prepared. One related phosphite complex, namely $[\text{W}(\text{CO})\{\text{P}(\text{OMe})_3\}(\eta\text{-PhC}\equiv\text{CMe})\text{Tp}]^+$, has been reported⁴ although the reaction of $[\text{W}(\text{CO})_2(\eta\text{-MeC}\equiv\text{CMe})\text{Tp}]^+$ **6**⁺ with $\text{P}(\text{OMe})_3$ in thf yielded an inseparable mixture of products, with IR carbonyl bands at 1876, 1911 and 1947 cm^{-1} , rather than $[\text{W}(\text{CO})\{\text{P}(\text{OMe})_3\}(\eta\text{-MeC}\equiv\text{CMe})\text{Tp}]^+$. (Earlier work showed that the reaction of $\text{P}(\text{OMe})_3$ with $[\text{W}(\text{CO})_2(\eta\text{-PhC}\equiv\text{CH})\text{Tp}]^+$ resulted in nucleophilic attack on the metal-bound alkyne carbon and subsequent loss of Me^+ to give the η^2 -vinyl complex $[\text{W}(\text{CO})_2\{\eta^2\text{-CPh}=\text{CHPO}(\text{OMe})_2\}\text{Tp}]$ [$\nu(\text{CO}) = 1880, 1968 \text{ cm}^{-1}$].⁹ The carbonyl bands at 1876 and 1947 cm^{-1} may therefore correspond to a similar product, *i.e.* $[\text{W}(\text{CO})_2\{\eta^2\text{-CMe}=\text{CMePO}(\text{OMe})_2\}\text{Tp}]$). The reaction of $[\text{Mo}(\text{CO})_2(\eta\text{-MeC}\equiv\text{CMe})\text{Tp}][\text{PF}_6]$ **3**⁺ $[\text{PF}_6]^-$ with $\text{P}(\text{OMe})_3$ in MeCN was also unsuccessful, leading only to the formation of $[\text{Mo}(\text{CO})(\text{NCMe})(\eta\text{-MeC}\equiv\text{CMe})\text{Tp}]^+$ **8**⁺, and in CHCl_3 a mixture of products was formed, probably including $[\text{MoCl}(\text{CO})(\eta\text{-MeC}\equiv\text{CMe})\text{Tp}]$.⁸

However, heating $[\text{W}(\text{CO})_2(\eta\text{-MeC}\equiv\text{CMe})\text{Tp}][\text{BF}_4]$ **6**⁺ $[\text{BF}_4]^-$ with $\text{P}(\text{OCH}_2)_3\text{CEt}$ {which cannot undergo the rearrangement observed with $\text{P}(\text{OMe})_3$ } in thf under reflux for 16 hours afforded a deep blue solution from which $[\text{W}(\text{CO})\{\text{P}(\text{OCH}_2)_3\text{CEt}\}(\eta\text{-MeC}\equiv\text{CMe})\text{Tp}][\text{BF}_4]$ **10**⁺ $[\text{BF}_4]^-$ was isolated as blue crystals on addition of *n*-hexane and cooling to $-20 \text{ }^\circ\text{C}$. The reaction appears to proceed *via* an associative pathway as IR carbonyl bands at 1866 and 1897 cm^{-1} are initially observed, consistent with the formation of $[\text{W}(\text{CO})_2\{\text{P}(\text{OCH}_2)_3\text{CEt}\}(\eta\text{-MeC}\equiv\text{CMe})\text{Tp}]^+$. The formation of such an intermediate, in which the alkyne would act as a two-electron donor, would facilitate substitution by an associative mechanism, as suggested for the related cyclopentadienyl complexes $[\text{Mo}(\text{CO})\text{L}(\eta\text{-RC}\equiv\text{CR})(\eta\text{-C}_5\text{H}_5)]^+$ (L = PET_3 , PCY_3 or PPh_3 ; $\text{R} = \text{R}' = \text{Me}$ or C_6H_5 , Me-4 , $\text{R} = \text{H}$, $\text{R}' = \text{Ph}$, Bu^1 or Pr^1).¹⁰

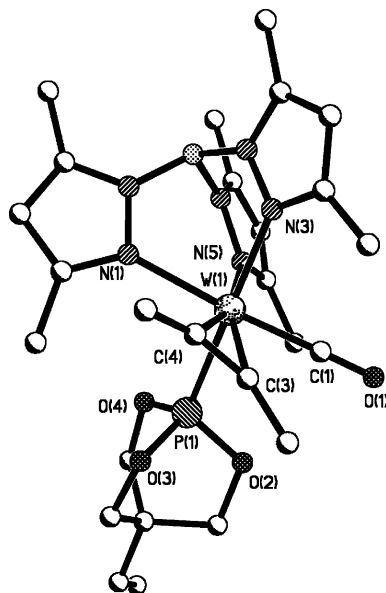
Table 4 Selected bond lengths (Å) and angles (°) for [W(CO){P(OCH₂)₃CEt}(η-MeC≡CMe)Tp][BF₄]·2CH₂Cl₂, **10**⁺[BF₄]⁻·2CH₂Cl₂

| | | | |
|----------------|----------|----------------|----------|
| W(1)–C(1) | 1.973(4) | W(1)–P(1) | 2.452(1) |
| W(1)–C(3) | 2.057(3) | C(3)–C(4) | 1.309(5) |
| W(1)–C(4) | 2.012(3) | C(1)–O(1) | 1.159(4) |
| P(1)–W(1)–C(1) | 85.3(1) | C(1)–W(1)–C(4) | 107.9(1) |
| P(1)–W(1)–C(3) | 82.0(1) | C(3)–W(1)–C(4) | 37.5(1) |
| P(1)–W(1)–C(4) | 95.0(1) | C(4)–C(3)–C(2) | 141.9(4) |
| C(1)–W(1)–C(3) | 71.9(1) | C(3)–C(4)–C(5) | 141.9(3) |
| β ^a | 16.9 | | |

^a β = the angle between the C≡C and M–C(O) vectors.

Attempts to prepare the analogous molybdenum complex [Mo(CO){P(OCH₂)₃CEt}(η-MeC≡CMe)Tp][PF₆] similarly in thf proved unsuccessful. However, the reaction of [Mo(CO)₂(η-MeC≡CMe)Tp][PF₆] **3**⁺[PF₆]⁻ with P(OCH₂)₃CEt in MeCN under reflux for 10 minutes, and subsequent purification using CH₂Cl₂-*n*-hexane, gave [Mo(CO){P(OCH₂)₃CEt}(η-MeC≡CMe)Tp][PF₆] **11**⁺[PF₆]⁻ as a green solid in moderate yield.

The complexes **10**⁺[BF₄]⁻ and **11**⁺[PF₆]⁻ were characterised by IR (Table 1) and NMR spectroscopy, cyclic voltammetry and, in the case of **10**⁺[BF₄]⁻·2CH₂Cl₂, by X-ray crystallography. The structure of the cation [W(CO){P(OCH₂)₃CEt}(η-MeC≡CMe)Tp]⁺ **10**⁺ is shown in Fig. 3 and important bond lengths and angles are given in Table 4. The tungsten coordination sphere is generally similar to that of **1**⁺[PF₆]⁻ with the W–C_{alkyne} bond distances {2.057(3) and 2.012(3) Å} again consistent with the alkyne acting as a four-electron donor.⁶ The alkyne is aligned approximately parallel to the carbonyl ligand {the angle, β, between the C≡C and W(CO) vectors is 16.9°} as in **1** and **1**⁺, (see above) and in other d⁴ species, e.g. the indenyl complex [Mo(CO)(PEt₃)(η-MeC≡CMe)(η⁵-C₉H₇)]⁺.¹⁰

**Fig. 3** The molecular structure of the cation [W(CO){P(OCH₂)₃CEt}(η-MeC≡CMe)Tp]⁺ **10**⁺. Hydrogen atoms have been omitted for clarity.

The ¹H and ¹³C-¹H} NMR spectra of **10**⁺ and **11**⁺ are similar to those of [W(CO){P(OMe)₃}(η-PhC≡CMe)Tp]⁺⁴ and the nitrile complexes **8**⁺ and **9**⁺, and are consistent with the asymmetric metal

centre. Again, the alkyne methyl resonances, at 2.75 and 3.51 ppm for **10**⁺ and at 2.83 and 3.46 for **11**⁺, are sharp suggesting that there is no alkyne rotation at room temperature, in contrast to fluxional [Mo(CO)(PR₃)(η-MeC≡CMe)(η-C₅H₅)]⁺ (R = Et, Cy or Ph) where the energy barrier to alkyne rotation increases as PR₃ becomes a better donor.¹⁰ Presumably the greater steric bulk of the Tp' ligand hinders such rotation. The ³¹P-¹H} NMR spectra of **10**⁺ and **11**⁺ show peaks at 131.9 and 139.5 ppm respectively, the former with satellites due to coupling to the ¹⁸³W nucleus (*I* = 1/2, 14%), with *J*(³¹P¹⁸³W) = 494 Hz.

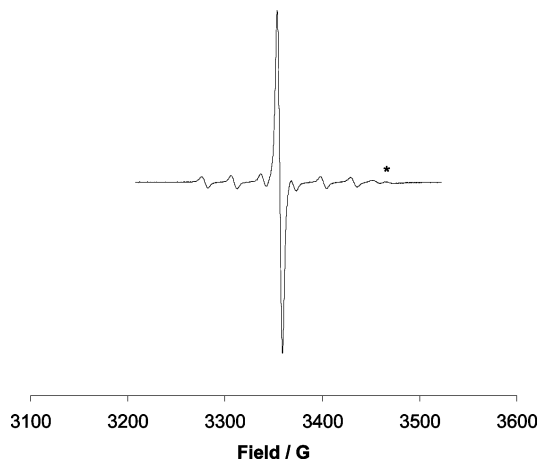
The CVs of **10**⁺ and **11**⁺ show reduction waves at -1.01 and -0.66 V, and oxidation waves at 1.28 and 1.39 V respectively; all are reversible and diffusion-controlled. The molybdenum complex, **11**⁺, is more easily reduced than the tungsten analogue by 0.35 V. The oxidation potential for **11**⁺ is lower than that of **10**⁺, albeit by only 0.11 V, but underlining the trend whereby the tungsten complex is more electron rich than the molybdenum complex.

Substitution of the carbonyl ligand in [M(CO)₂(η-MeC≡CMe)Tp]⁺ by P(OCH₂)₃CEt results in the reduction wave shifting to more negative potentials by ca. 0.5 V, mirroring the trend observed for the chromium(i) cations, [Cr(CO)L(η-RC≡CR)(η-C₆Me₆)]⁺ {L = CO and P(OR)₃}.² However, the shift is less than observed for carbonyl substitution by the better donor, MeCN.

ESR spectroscopy of [M(CO)L(η-RC≡CR)Tp]⁺ {L = CO or P(OCH₂)₃CEt}

As noted above, all of the complexes [M(CO)L(η-MeC≡CMe)Tp]⁺ undergo one-electron reduction to the neutral molecules [M(CO)L(η-MeC≡CMe)Tp]. For L = MeCN, the reduced form is unstable, giving [MCl(CO)(η-MeC≡CMe)Tp] in CH₂Cl₂. However, for L = CO and P(OCH₂)₃CEt the paramagnetic species are stable enough to be studied by ESR spectroscopy.

The room temperature, fluid solution ESR spectrum of the isolated complex [Mo(CO)₂L(η-PhC≡CPh)Tp]⁺ **1** in toluene is shown in Fig. 4. The spectra of **2**–**7** are qualitatively similar (Table 2) and were obtained *in situ* by reducing the corresponding diamagnetic cations with [Co(η-C₅H₅)₂] in toluene or, in the case of **5**, by

**Fig. 4** Fluid solution ESR spectrum of the isolated complex [Mo(CO)₂(η-PhC≡CPh)Tp]⁺ **1** in toluene. The asterisk indicates an impurity.

reducing the cation **5**⁺ in CH₂Cl₂, evaporating the reaction mixture to dryness, and extracting the paramagnetic product into toluene.

The isotropic spectra of the molybdenum complexes **1–4** consist of a central line ($g_{\text{iso}} = 2.007\text{--}2.011$) flanked by ^{95,97}Mo satellites ($I = 5/2$, 25.5% combined natural abundance) with $A_{\text{iso}}(^{95,97}\text{Mo})$ ca. 30 G (Table 2). The tungsten analogues **5–7** show relatively broad isotropic spectra ($g_{\text{iso}} = 2.016\text{--}2.021$), with resolved ¹⁸³W satellites ($I = 3/2$, 14.3% natural abundance). ¹H coupling was not observed for the PhC≡CH complexes **4** and **7**, in contrast to the 4.2 G coupling observed previously for [Cr(CO)₂(η-PhC≡CH)(η-C₆Me₆)]⁺.² Spectra of the phosphite-containing analogues, [W(CO){P(OCH₂)₃CEt}(η-MeC≡CMe)Tp]⁺ **10** and [Mo(CO){P(OCH₂)₃CEt}(η-MeC≡CMe)Tp]⁺ **11**, were obtained by reducing the cations **10**⁺ and **11**⁺ with [Co(η-C₅Me₅)₂] and [Co(η-C₅H₅)₂] respectively in CH₂Cl₂ : thf (1 : 2). The isotropic ESR spectra of **10** and **11** (Fig. 5) show coupling of the unpaired electron to ³¹P ($I = 1/2$, 100%) in addition to the metal nuclei.

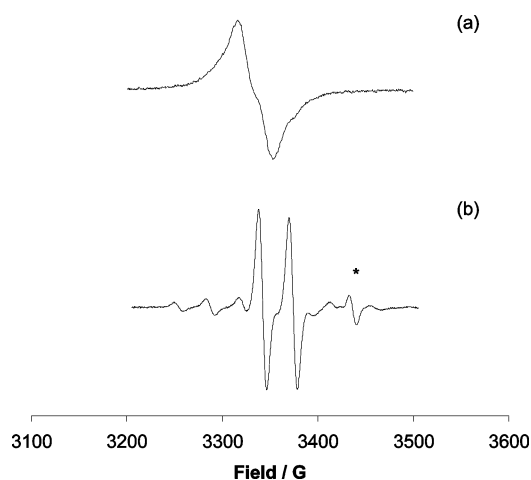


Fig. 5 Fluid solution ESR spectra of (a) [Mo(CO){P(OCH₂)₃CEt}(η-MeC≡CMe)Tp]⁺ **11** and (b) [W(CO){P(OCH₂)₃CEt}(η-MeC≡CMe)Tp]⁺ **10** in CH₂Cl₂ : thf (1 : 2). The asterisk indicates an impurity.

Frozen toluene solutions of **1–7** reveal rhombic g -values with associated hyperfine satellites. Example spectra, of complexes **3** and **6**, are shown in Fig. 6. Complexes **10** and **11** behave similarly with additional splitting to ³¹P (Fig. 7).

Simulations. The fluid and frozen solution ESR spectra were simulated for [Mo(CO)₂(η-MeC≡CMe)Tp]⁺ **3**, [W(CO)₂(η-MeC≡CMe)Tp]⁺ **6**, [W(CO){P(OCH₂)₃CEt}(η-MeC≡CMe)Tp]⁺ **10** and [Mo(CO){P(OCH₂)₃CEt}(η-MeC≡CMe)Tp]⁺ **11**, complexes with a common coordinated alkyne (MeC≡CMe), in order to probe the electronic structure. (Simulations of the spectra of [Mo(CO)₂(η-PhC≡CPh)Tp]⁺ gave very similar parameters to those of **3**, so the nature of the alkyne appears to have little influence.) The spectra of the tungsten complexes **6** and **10** could be simulated assuming simple rhombic models (*i.e.* $x \neq y \neq z$, but the principal axes of the g and A matrices are coincident with each other and with the molecular axis system) with the parameters in Table 5. These two complexes have near axial ¹⁸³W hyperfine matrices with ‘unique’, large A_3 -values [Fig. 6(b) and 7(b)]. Note that there are additional features in the spectrum of **10** that cannot be reproduced—these are due to an impurity, as is also observed in the fluid solution spectrum.

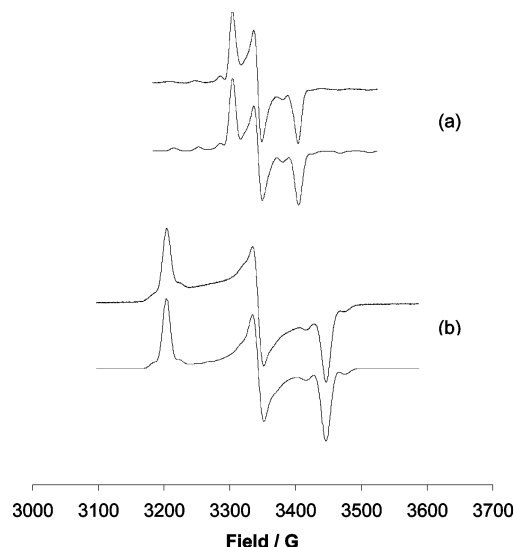


Fig. 6 Frozen toluene solution ESR spectra of (a) [Mo(CO)₂(η-MeC≡CMe)Tp]⁺ **3** and (b) [W(CO)₂(η-MeC≡CMe)Tp]⁺ **6** at 77 K. In each case, the upper spectrum is experimental and the lower spectrum is the simulation using the parameters described in the text with Gaussian line widths of $W_1 = 11$, $W_2 = 8$, $W_3 = 10$ G (**3**) and $W_1 = W_2 = 11$, $W_3 = 10$ G (**6**).

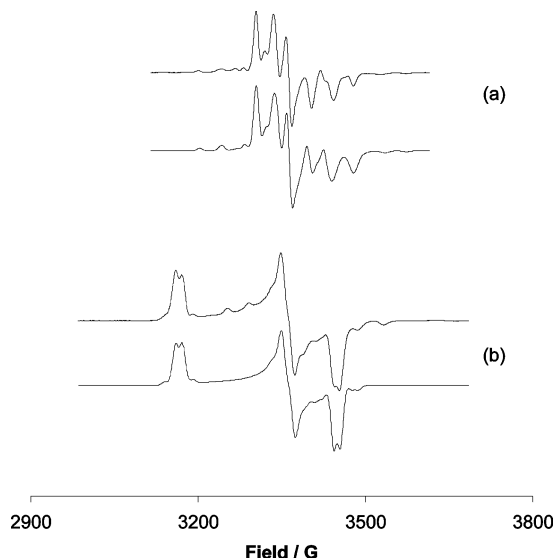


Fig. 7 Frozen CH₂Cl₂ : thf (1 : 2) solution ESR spectra of (a) [Mo(CO){P(OCH₂)₃CEt}(η-MeC≡CMe)Tp]⁺ **11** at 120 K and (b) [W(CO){P(OCH₂)₃CEt}(η-PhC≡CPh)Tp]⁺ **10** at 110 K. In each case, the upper spectrum is experimental and the lower spectrum is the simulation using the parameters described in the text with Gaussian line widths of $W_1 = W_2 = 9$, $W_3 = 15$ G (**11**) and $W_1 = 12$, $W_2 = W_3 = 14$ G (**10**).

Initial attempts to simulate the frozen solution ESR spectra of the Mo complexes **3** and **11** used a simple rhombic model similar to that for the W analogues. Although these gave reasonable fits, there were notable discrepancies in the positions of the hyperfine transitions (and the line shapes) on the low-field shoulders of g_1 and between g_2 and g_3 . In addition, the patterns of the hyperfine coupling constants obtained (two large values and one small value, with the ‘unique’ value corresponding to the middle g -value) were not consistent with the unpaired electron in one of the t_{2g} orbitals.

Table 5 ESR simulation parameters for $[M(\text{CO})L(\eta\text{-MeC}\equiv\text{CMe})\text{Tp}']$ $\{M = \text{Mo}, L = \text{CO } \mathbf{3}$ or $\text{P}(\text{OCH}_2)_3\text{CEt } \mathbf{11}$; $M = \text{W}, L = \text{CO } \mathbf{6}$ or $\text{P}(\text{OCH}_2)_3\text{-CEt } \mathbf{10}\}$

| | g_{iso} | g_1 | g_2 | g_3 | $A_{\text{iso(M)}}^a$ | $A_{1(\text{M})}$ | $A_{2(\text{M})}$ | $A_{3(\text{M})}$ | a^b | $A_{\text{iso(P)}}^c$ | $A_{1(\text{P})}^c$ | $A_{2(\text{P})}$ | $A_{3(\text{P})}$ |
|-----------|------------------|-------|-------|-------|-----------------------|-------------------|-------------------|-------------------|-------|-----------------------|---------------------|-------------------|-------------------|
| 3 | 2.011 | 2.039 | 2.016 | 1.979 | 31.1 | +19 | +22 | +44 | 35 | — | — | — | — |
| 11 | 2.001 | 2.027 | 1.990 | 1.944 | 35 | +19 | +23 | +44 | 50 | 32 | 25 | 35 | 31 |
| 6 | 2.021 | 2.102 | 2.015 | 1.955 | 42 | -37 | -38 | -53 | — | — | — | — | — |
| 10 | 2.015 | 2.126 | 2.002 | 1.951 | ^d | -40 | -36 | -59 | — | 19 | 11 | 11 | 11 |

^a A in 10^{-4} cm^{-1} . ^b Monoclinic model with twist about g_2/A_2 axis of a° . ^c Modelled with P hyperfine axes coincident with g -matrix principal axes. ^d Not resolved.

For these low spin d^5 complexes one would expect one hyperfine coupling to be significantly larger than the other two and to correspond to the smallest g -value ($< g_2$) (see below), as observed for the W complexes **6** and **10** (see above). Therefore, the possibility of non-coincidence effects, and reducing the symmetry to monoclinic (*i.e.* one of the g and A axes is coincident, with the other two rotated through an angle a), was investigated. If the axis of rotation is such that a numerically large hyperfine value is mixed with a small value, this can have the effect of producing two apparently numerically similar values in the observed spectrum. Introducing an angle of twist a about g_2/A_2 will thus mix A_1 and A_3 .

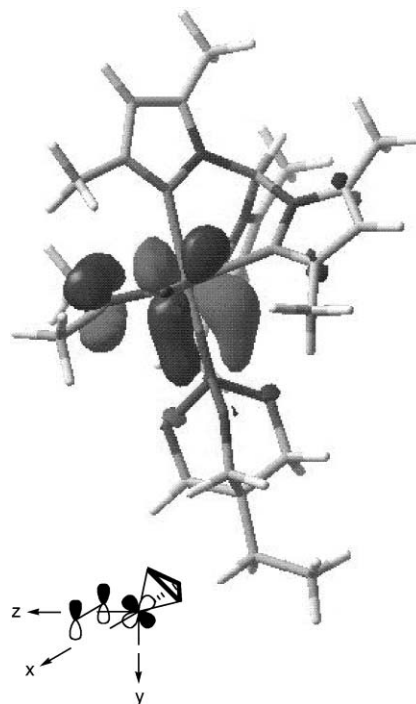
A process of trial and error gave the best fit parameters in Table 5. A significant twist of $a = 35^\circ$ is found for $[\text{Mo}(\text{CO})_2(\eta\text{-MeC}\equiv\text{CMe})\text{Tp}']$ **3**, with a small value of A_1 and a larger value of A_3 . Thus, the diagonal A -matrix is now near-axial with a “unique” large A -value, associated with the smallest g -value, as expected for low spin d^5 . This model gives a much better fit to the experimental spectrum than the simple rhombic model [Fig. 6(a)]. For complex $[\text{Mo}(\text{CO})\{\text{P}(\text{OCH}_2)_3\text{CEt}\}(\eta\text{-MeC}\equiv\text{CMe})\text{Tp}']$ **11**, a similar process was followed as for **3**. Initially, only the g -matrix and ^{31}P hyperfine matrix were considered. The ^{31}P hyperfine is near-axial about A_2 , and the spectra were not sensitive to non-coincidence between the g and ^{31}P A -matrices. After these parameters were set the Mo-hyperfine matrix was included; again a noticeably better fit is found for a monoclinic model [Fig. 7(a), parameters in Table 5].

It should be noted that there are other sets of parameters that give reasonable simulations of **3** and **11** in a monoclinic model. For example, a simulation of the spectrum of **11** using genetic algorithm methods to optimise the parameters,¹¹ gives the best fit parameters with $g_1 = 2.012$, $g_2 = 2.029$, $g_3 = 1.949$, $A_{1(\text{Mo})} = 26.0 \text{ G}$, $A_{2(\text{Mo})} = 40.2 \text{ G}$, $A_{3(\text{Mo})} = 36.2 \text{ G}$, $A_{1(\text{P})} = 26.2 \text{ G}$, $A_{2(\text{P})} = 37.3 \text{ G}$, $A_{3(\text{P})} = 37.5 \text{ G}$, and a monoclinic twist of 35.6° about g_1/A_1 . The principal g and $A_{(\text{Mo})}$ values are similar to those obtained from a simple rhombic model (two large and one small metal hyperfine) highlighting the fact that mixing two numerically similar A -values has little effect on the observed spectrum. Moreover, these complexes do *not* have monoclinic symmetry—their true symmetry is lower which could in principle lead to triclinic ESR symmetry (non-coincidence between all three axes of the g/A -matrices). However, the spectra can be fitted well with a single twist and do not justify including further fitting parameters. We therefore restrict ourselves to the simpler model, preferring the solution using the parameters in Table 5, as the values are intuitively more sensible. Simulations of the spectra of the W complexes **6** and **10** proved to be insensitive to non-coincidence effects, which is not unexpected as such effects are

more apparent for larger values of the nuclear spin quantum number I . It is possible that there is non-coincidence in these systems and that it is simply not detectable in the frozen solution ESR spectra.

Analysis. For all of the complexes $[\text{Mo}(\text{CO})_2(\eta\text{-MeC}\equiv\text{CMe})\text{Tp}']$ **3**, $[\text{W}(\text{CO})_2(\eta\text{-MeC}\equiv\text{CMe})\text{Tp}']$ **6**, $[\text{W}(\text{CO})\{\text{P}(\text{OCH}_2)_3\text{CEt}\}(\eta\text{-MeC}\equiv\text{CMe})\text{Tp}']$ **10** and $[\text{Mo}(\text{CO})\{\text{P}(\text{OCH}_2)_3\text{CEt}\}(\eta\text{-MeC}\equiv\text{CMe})\text{Tp}']$ **11** the principal values of the diagonal metal hyperfine matrices average well to the experimentally observed isotropic value. Therefore, in each complex $A_{1(\text{M})}$, $A_{2(\text{M})}$, $A_{3(\text{M})}$ and $A_{\text{iso(M)}}$ have the same sign. The same is also true of the ^{31}P couplings in **10** and **11**. The absolute signs of the metal hyperfine components arise from the analysis below.

In the Mo complexes, the coordinated alkyne tends to align more with one CO than the other (see above). As shown below, DFT calculations predict that the SOMO in this case is primarily M d_{yz} based where z is defined by the M–C₂ direction, x is along the M–CO bond co-parallel to the alkyne C≡C bond, and y is along the M–P or second M–CO axis (Fig. 8).

**Fig. 8** The SOMO and coordinate system of $[\text{M}(\text{CO})L(\eta\text{-MeC}\equiv\text{CMe})\text{Tp}']$.

If the sole metal contribution to the SOMO is the d_{yz} orbital, one would expect the system to have rhombic ESR symmetry with A_x the largest component of the hyperfine matrix.¹² For a d_{yz} ground state in a t_{2g}^5 system one would also expect¹² one g -value (g_x) below the free electron value g_e and two larger (g_y, g_z), as observed experimentally. Thus, g_3 and A_3 can be confidently assigned as g_x and A_x , respectively, for all the complexes. If a is the LCAO coefficient of the d_{yz} orbital in the SOMO, one can then derive a^2 from eqn (1):

$$A_x - \langle A \rangle = P_d \left[-\frac{4}{7}a^2 + \frac{2}{3}\Delta g_x - \frac{5}{42}(\Delta g_y + \Delta g_z) \right] \quad (1)$$

where $\langle A \rangle = (A_x + A_y + A_z)/3$, and the Δg terms are the shifts of the g -values from g_e .

Substituting the values in Table 5 for the tungsten complexes **6** and **10** (in this analysis Y and Z do not need to be assigned) with $P_d = +57.9 \times 10^{-4} \text{ cm}^{-1}$ for **W**, calculated using Rieger's methodology for a $5d^5$ configuration,¹³ one obtains $a^2 = 0.22$ and 0.33 for **6** and **10**, respectively. Note that sensible answers (positive values of a^2) are only obtained for hyperfine couplings having negative sign. Thus, the SOMO is only 20–30% localised on the metal d-orbitals, with the phosphite complex **10** having greater metal character in the SOMO which presumably reflects the greater electron withdrawing nature of the CO ligand *cf.* the phosphite.

The non-coincidence effects between the principal axes of the diagonal g and A_{Mo} matrices in **3** and **11** must arise from mixing of d-orbitals in the SOMO. A possible cause of the non-coincidence effects here could be a rotation of the alkyne about z , which could mix d_{yz} with d_{xz} in the SOMO. This is supported by the DFT calculations on **3**, **6**, **10** and **11**, which show that the only other significant metal contribution to the SOMO is indeed d_{xz} . In the analysis of the Mo hyperfine couplings, it is assumed that $|\text{SOMO}\rangle = a|yz\rangle + b|xz\rangle$ where $a > b$. Mixing these two orbitals requires a rotation about the molecular z -axis, and thus (*vide supra*) g_2 and A_2 are labelled as g_z and A_z . If $a > b$ (*i.e.* the d_{yz} orbital is dominant) then the largest component of the metal hyperfine (A_3) is expected to be A_x as before (see below). This leaves g_1, A_1 as g_y, A_y . (Note that here X and Y refer to the non-coincident principal axes of the diagonal g and A -matrices and are therefore not a consistent axis system—twisting through a about Z , which is common to both sets of axes and to the molecular axes, interconverts them.)

In this case the non-zero elements of the metal hyperfine matrix are expected to be [ignoring spin-orbit coupling terms (g -shifts) for simplicity]:

$$\begin{aligned} A_{xx} &= A_s + \frac{2}{7}P_d(-2a^2 + b^2) \\ A_{yy} &= A_s + \frac{2}{7}P_d(a^2 - 2b^2) \\ A_{zz} &= A_s + \frac{2}{7}P_d(a^2 + b^2) \\ A_{xy} &= A_s + \frac{2}{7}P_d(3ab) \end{aligned}$$

where A_s is the Fermi contact term. This matrix can be diagonalised by rotation about z by an angle a such that:¹²

$$\tan a = \frac{-2\sqrt{R}}{1 - R} \quad (2)$$

where $R = b^2/a^2$ (*i.e.* the hybridisation ratio). This give the diagonal terms:

$$\begin{aligned} A_x &= A_s - \frac{4}{7}P_d(a^2 + b^2) \\ A_y &= A_s + \frac{2}{7}P_d(a^2 + b^2) \\ A_z &= A_s + \frac{2}{7}P_d(a^2 + b^2) \end{aligned}$$

and hence,

$$A_x - \langle A \rangle = -\frac{4}{7}P_d(a^2 + b^2) \quad (3)$$

Substitution of the data in Table 5 into eqn (3) for $[\text{Mo}(\text{CO})_2(\eta\text{-MeC}\equiv\text{CMe})\text{Tp}]$ **3** and $[\text{Mo}(\text{CO})\{\text{P}(\text{OCH}_2)_3\text{CEt}\}(\eta\text{-MeC}\equiv\text{CMe})\text{Tp}]$ **11** (with $P_d = -51.9 \times 10^{-4} \text{ cm}^{-1}$ calculated for Mo with a $4d^5$ configuration)¹³ gives the total metal d-orbital contributions to the SOMO ($a^2 + b^2$) = 0.53 and 0.51, respectively. Including approximate corrections for spin-orbit coupling makes little difference to these values because of the small experimentally observed g -shifts. Note that sensible answers are only obtained for hyperfine couplings having positive sign. Substitution of the experimental angles of non-coincidence in to eqn (2) gives the hybridisation ratios $b^2/a^2 = 0.10$ and 0.22 for **3** and **11**, respectively. Thus, in **3** the SOMO is 48% d_{yz} and 5% d_{xz} , and in **11** the SOMO is 42% d_{yz} and 9% d_{xz} . It should be borne in mind that, because of the ambiguities in the simulation of the spectra of **3** and **11** (see above), these $a^2 + b^2$ values should probably be treated as identical within the accuracy of the analysis.

The ^{31}P hyperfine coupling for $[\text{W}(\text{CO})\{\text{P}(\text{OCH}_2)_3\text{CEt}\}(\eta\text{-MeC}\equiv\text{CMe})\text{Tp}]$ **10** is isotropic within the resolution of the spectra, meaning that the P 3p orbital contribution to the SOMO must be very small. However, in **11** the largest component of the anisotropic hyperfine couplings is A_2 , which is A_z following the assignment of the g -values and metal hyperfine couplings and using the same coordinate system. This implies a $3p_z$ contribution to the SOMO, which can mix with the Mo $4d_{yz}$ orbital, and this is supported by the DFT calculations (see below and Fig. 8). This contribution can be quantified from:

$$A_z - \langle A \rangle = \frac{4}{5}P_p c^2$$

where c is the LCAO coefficient of the P $3p_z$ in the SOMO and $P_p = +306 \times 10^{-4} \text{ cm}^{-1}$,¹⁴ to give $c^2 = 0.02$, *i.e.* a 2% contribution to the SOMO of **11**.

DFT calculations on $[\text{Mo}(\text{CO})_2(\eta\text{-MeC}\equiv\text{CMe})\text{Tp}]$ **3**, $[\text{W}(\text{CO})_2(\eta\text{-MeC}\equiv\text{CMe})\text{Tp}]$ **6**, $[\text{W}(\text{CO})\{\text{P}(\text{OCH}_2)_3\text{CEt}\}(\eta\text{-MeC}\equiv\text{CMe})\text{Tp}]$ **10** and $[\text{Mo}(\text{CO})\{\text{P}(\text{OCH}_2)_3\text{CEt}\}(\eta\text{-MeC}\equiv\text{CMe})\text{Tp}]$ **11**

In order to understand further the results of the ESR analysis, DFT calculations have been carried out on $[\text{Mo}(\text{CO})_2(\eta\text{-MeC}\equiv\text{CMe})\text{Tp}]$ **3**, $[\text{W}(\text{CO})_2(\eta\text{-MeC}\equiv\text{CMe})\text{Tp}]$ **6**, $[\text{W}(\text{CO})\{\text{P}(\text{OCH}_2)_3\text{CEt}\}(\eta\text{-MeC}\equiv\text{CMe})\text{Tp}]$ **10** and $[\text{Mo}(\text{CO})\{\text{P}(\text{OCH}_2)_3\text{CEt}\}(\eta\text{-MeC}\equiv\text{CMe})\text{Tp}]$ **11**, with the same coordinate system as used in the ESR analysis. The geometries of the neutral compounds were optimised as unrestricted spin-doublets using

Table 6 X-Ray crystallographically determined bond lengths (Å) and the angle, β , between the C \equiv C and W–C(O) vectors for [W(CO){P(OCH₂)₃CEt}(η -MeC \equiv CMe)Tp]⁺ **10**⁺, and calculated values for both **10**⁺ and **10**

| | W–X ^a | C \equiv C | W–P | M–CO | C \equiv O | β /° |
|-------------------------------------|------------------|--------------|-------|-------|--------------|------------|
| 10 ⁺ (X-ray) | 1.927 | 1.309 | 2.452 | 1.973 | 1.159 | 16.9 |
| 10 ⁺ (calculated) | 1.944 | 1.322 | 2.505 | 1.999 | 1.160 | 17.4 |
| 10 (calculated) | 2.072 | 1.289 | 2.378 | 1.970 | 1.173 | 13.4 |

^a X = midpoint of C \equiv C bond.

B3LYP density functional theory implemented by the programme Jaguar,¹⁵ with the 6–31G* basis set for non-metals and LACV3P¹⁶ for the metal atom. This optimised geometry was then used as the basis for a natural bond orbital (NBO) analysis,¹⁷ which gave the total spin population on each atom and a breakdown of the SOMO into contributions from each atomic orbital. For the purposes of comparison with the crystallographic study, the structure of **10**⁺ was calculated using the same methods.

Table 6 compares the crystallographically determined bond lengths of **10**⁺ with those calculated for **10** and **10**⁺. There is good agreement between the calculated and structurally determined metrics of **10**⁺, especially as the calculated structure is of an isolated gas-phase ion. The calculated changes in the metal–alkyne unit upon reduction of **10**⁺ to **10** are in agreement with those predicted by the bonding model from ref. 2 in that the orbital depopulated upon oxidation is metal–alkyne antibonding.

In all cases, the unpaired electron is located mainly in the d_{yz} orbital of the metal (again, consistent with the MO scheme from ref. 2, and in agreement with this being the major metal contribution to the SOMO from the analysis of the ESR spectra). The second largest contribution is from the metal d_{xz} orbital; no other atomic orbital contains more than 4% of the unpaired electron. Table 7 lists pertinent values. More electron density resides on the molybdenum atoms than on the tungsten atoms, and this is also reflected in the greater amount of spin population of the phosphorus p_z orbital for **10** compared to **11**. The total spin population on the metal atom increases upon replacing a carbonyl ligand with a phosphite, as would be expected on replacing a good π -acceptor with a poorer π -acceptor. For the molybdenum compounds **3** and **11**, the ratio of the d_{xz} contribution to that of the d_{yz} is approximately 0.17, whereas for **6** and **10** it is about 0.10. This is consistent with the computed values of β {the angle between the C \equiv C and M–C(O) vectors}, because it is the breaking of the local symmetry by a rotation of the alkyne that allows mixing of the two orbitals, and the molybdenum compounds have larger values of β . The larger calculated value of β for **11** *cf.* **3** is also consistent with the larger angle of non-coincidence (α) found between the *g* and Mo hyperfine matrices for **11** if the rotation of the alkyne about

the M–C₂ direction is the mechanism for mixing the d_{yz} and d_{xz} orbitals in the SOMO.

One striking feature is that, although the trends are in agreement, the computationally calculated metal spin populations are considerably larger than those from the ESR spectroscopic data. The d_{yz} contribution to the SOMO is computed at 57% and 66% for **3** and **11** respectively, compared to values from the ESR analysis of 48% and 42%. The analogous values for **6** and **10** are calculated at 47% and 61%, compared to 22% and 33% from the ESR spectra. Clearly, there is a significant discrepancy between the two approaches, with either the calculated values being too large or the ESR values being too small (or, probably more likely, both, with the real values lying between those from the two approaches).

A comparison of the calculated and crystallographic structures of **10**⁺ indicates one possible source of error. The computed metal–phosphite distance is too long (which is recognised to be a problem when comparing crystallographically determined structures with gas-phase calculations¹⁸) which, since the ligand is a π -acceptor, might imply that the model system has not included sufficient π back-donation. If this were also the case for the neutral compounds, then the computations would indicate too much unpaired electron density in the d_{yz} orbitals, as seems to be the case for all compounds. It would also indicate too little electron density in the phosphorus p_z orbital of **10** and **11**, leading to a computed value of about 1% for **11** compared with the value from the ESR spectrum of about 2%. However, the apparent margin of disagreement about the phosphorus p_z occupancy (approximately 1% between the two methods) is an order of magnitude smaller than the disagreement over the metal d_{yz} occupancy (24 to 29%), and it seems unlikely that correcting the former would resolve the latter. It is worth noting at this point that the calculation of metal hyperfine coupling constants using conventional basis sets (such as that used here) is recognised to be problematic (because of the form at the nucleus of the Gaussian orbitals used).¹⁹

A second possible source of error might be the simplifying assumptions used in the ESR spectroscopic analysis, in particular that the metal orbital contribution to the SOMO is either purely d_{yz} or a d_{yz}/d_{xz} hybrid; the symmetry at the metal is undoubtedly lower than assumed, and there are therefore contributions to the SOMO from the remaining d orbitals. Hence, although modelling the spectra as rhombic or monoclinic gives good fits to the experimental data, it neglects some small effects.

Conclusions

The dicarbonyls [M(CO)₂(η -RC \equiv CR')Tp]⁺ {M = Mo or W, Tp' = hydrotris(3,5-dimethylpyrazolyl)borate} undergo one-electron reduction to paramagnetic [M(CO)₂(η -RC \equiv CR')Tp]⁰; structural studies on the redox pair [Mo(CO)₂(η -PhC \equiv CPh)Tp]^z (z = 0 and

Table 7 NBO calculated spin populations (%) for [M(CO)₂L(η -MeC \equiv CMe)Tp]⁺ {M = Mo, L = CO **3** or P(OCH₂)₃CEt **11**; M = W, L = CO **6** or P(OCH₂)₃CEt **10**}, and β , the angle between the C \equiv C and M–C(O) vectors

| | Total metal unpaired electron density | Metal d _{yz} | Metal d _{xz} | d _{xz} /d _{yz} | Phosphorus p _z | β /° |
|-----------|---------------------------------------|-----------------------|-----------------------|----------------------------------|---------------------------|------------|
| 3 | 0.735 | 0.569 | 0.098 | 0.17 | — | 15.7 |
| 6 | 0.580 | 0.470 | 0.043 | 0.09 | — | 9.5 |
| 10 | 0.740 | 0.605 | 0.065 | 0.11 | 0.037 | 13.4 |
| 11 | 0.848 | 0.657 | 0.118 | 0.18 | 0.011 | 17.7 |

1) show reduction is accompanied by a lengthening of the Mo–C_{alkyne} bonds, and a shortening of the C≡C bond, consistent with conversion of a three- to a four-electron donating alkyne ligand.

Substitution of one carbonyl ligand of [M(CO)₂(η-R₂C≡CR')Tp]⁺ gives [M(CO)L(η-R₂C≡CR')Tp]⁺ {L = MeCN or P(OCH₂)₃CEt}, the reduction potentials of which are significantly more negative. Chemical reduction of the nitrile complex [Mo(CO)(NCMe)(η-MeC≡CMe)Tp][PF₆] results in the formation of [MoCl(CO)(η-MeC≡CMe)Tp] in CH₂Cl₂ whereas more stable paramagnetic phosphite complexes, [M(CO){P(OCH₂)₃-CEt}(η-R₂C≡CR')Tp], have been characterised by ESR spectroscopy. The ESR spectroscopic results illustrate that the SOMO of the neutral, d⁵ species (the LUMO of the cationic d⁴ species) are considerably more delocalised for the tungsten than for the molybdenum complexes, in agreement with DFT calculations. Furthermore, they support a decrease in electron density at the metal on replacement of CO with the poorer π-acceptor phosphite ligand. The ESR spectra of the Mo species also reveal non-coincidence effects between the *g* and metal hyperfine matrices, a possible mechanism for which is a rotation of the coordinated alkyne about the M–C₂ axis, and consequent mixing of the metal d-orbitals.

Experimental

The preparation, purification and reactions of the complexes described were carried out under an atmosphere of dry nitrogen, using dried and deoxygenated solvents purified either by distillation or by using Anhydrous Engineering double alumina or alumina/copper catalyst drying columns. Reactions were monitored by IR spectroscopy where necessary. Unless stated otherwise complexes were purified by dissolution in CH₂Cl₂, filtration of the solution through Celite, addition of *n*-hexane to the filtrate, and reduction of the volume of the mixture *in vacuo* to induce precipitation.

The compounds [M(CO)₃Tp] (M = Mo, W),²⁰ [W(CO)₂(η-R₂C≡CR')Tp][PF₆] (R = R' = Me, Ph; R = Ph, R' = H),⁴ [W(CO)₃Tp],⁴ [Fe(η-C₅H₅)₂][PF₆],²¹ [Fe(η-C₅H₅)(η-C₅H₄COMe)][BF₄],²¹ [Co(η-C₅H₅)₂]²² and [Co(η-C₅Me₅)₂]²³ were prepared by published methods.

IR spectra were recorded on a Nicolet 5ZDX FT spectrometer or a Perkin Elmer Spectrum One FT-IR spectrometer fitted with a Perkin Elmer ZnSe Universal ATR sampling accessory. Proton, ³¹P and ¹³C-{¹H} NMR spectra were recorded on JEOL GX270, GX400 or λ300 spectrometers with SiMe₄ (¹H and ¹³C) or H₃PO₄ (³¹P) as internal standards. X-Band ESR spectra were recorded on a Bruker ESP300 spectrometer equipped with a Bruker variable temperature accessory and a Hewlett-Packard 5350B microwave frequency counter. The field calibration was checked by measuring the resonance of the diphenylpicrylhydrazyl (dpph) radical before each series of spectra. Electrochemical studies were carried out using an EG&G model 273A potentiostat in conjunction with a three-electrode cell. The auxiliary electrode was a platinum wire and the working electrode a platinum disc (1.6 or 2.0 mm diameter). The reference was an aqueous saturated calomel electrode separated from the test solution by a fine porosity frit and an agar bridge saturated with KCl. Solutions were 1.0 × 10⁻³ mol dm⁻³ in the test compound and 0.1 mol dm⁻³ in [NBuⁿ][PF₆] as the supporting electrolyte in CH₂Cl₂. Under

the conditions used, *E*^{o'} for the one-electron oxidation of [Fe(η-C₅H₅)₂] or [Fe(η-C₅Me₅)₂] and the one-electron reduction of [Co(η-C₅H₅)₂][BF₄], added to the test solutions as internal calibrants, is 0.47, -0.08 and -0.86 V respectively in CH₂Cl₂.

Microanalyses were carried out by the staff of the Microanalysis Service of the School of Chemistry, University of Bristol.

Syntheses

[Mo(CO)₂(η-PhC≡CPh)Tp][PF₆]·CH₂Cl₂, 1⁺[PF₆]⁻·CH₂Cl₂. To a stirred solution of [Mo(CO)₃Tp] (2.0 g, 4.19 mmol) and PhC≡CPh (1.50 g, 8.42 mmol) in CH₂Cl₂ (100 cm³) was added [Fe(η-C₅H₅)₂][PF₆] (1.38 g, 4.17 mmol). The dark brown solution was heated under reflux for 24 h. The solvent was removed *in vacuo* leaving a red solid which was washed thoroughly with diethyl ether (4 × 50 cm³) to remove [Fe(η-C₅H₅)₂] and PhC≡CPh. The residue was redissolved in CH₂Cl₂ (20 cm³) and filtered through Celite. Addition of diethyl ether (50 cm³) and cooling to -20 °C induced precipitation of a red powder. A second purification using CH₂Cl₂-diethyl ether gave the product as the crimson-red crystalline 1 : 1 CH₂Cl₂ solvate, yield 2.16 g (60%).

The complex [Mo(CO)₂(η-4-MeOC₆H₄C≡CC₆H₄OMe-4)Tp][PF₆].0.5CH₂Cl₂, 2⁺[PF₆]⁻.0.5CH₂Cl₂ was prepared similarly in 65% yield, but only required the reaction mixture to be heated under reflux for 4 h.

[Mo(CO)₂(η-MeC≡CMe)Tp][PF₆], 3⁺[PF₆]⁻. To a stirred solution of [Fe(η-C₅H₅)₂][PF₆] (0.69 g, 2.08 mmol) and MeC≡CMe (0.5 cm³, 6.38 mmol) in CH₂Cl₂ (50 cm³) was added [Mo(CO)₃Tp] (1.0 g, 2.10 mmol). After 45 min the solvent was removed *in vacuo* leaving a green solid which was washed thoroughly with diethyl ether (3 × 25 cm³) to remove [Fe(η-C₅H₅)₂] and any residual MeC≡CMe. The residue was redissolved in CH₂Cl₂ (20 cm³) and filtered through Celite. Toluene (50 cm³) was added and the volume of the mixture reduced *in vacuo*, inducing the precipitation of a green powder. A second purification using CH₂Cl₂-diethyl ether gave the product as a green crystalline solid, yield 0.82 g (60%).

[Mo(CO)₂(η-PhC≡CH)Tp][PF₆].CH₂Cl₂, 4⁺[PF₆].CH₂Cl₂. To a stirred solution of [Mo(CO)₃Tp] (1.00 g, 2.10 mmol) and PhC≡CH (0.5 cm³, 4.51 mmol) in CH₂Cl₂ (50 cm³) was added [Fe(η-C₅H₅)₂][PF₆] (0.69 g, 2.09 mmol). After 20 min the dark brown solution was evaporated to dryness *in vacuo*. The brown residue was washed thoroughly with diethyl ether (3 × 25 cm³) to remove [Fe(η-C₅H₅)₂] and residual PhC≡CH. The residue was redissolved in CH₂Cl₂ and filtered through Celite. Addition of diethyl ether (50 cm³) and cooling to -20 °C induced precipitation of a brown powder. A second purification using CH₂Cl₂-diethyl ether gave the product as the orange-brown crystalline 1.0 CH₂Cl₂ solvate, yield 0.65 g (40%).

[Mo(CO)₂(η-PhC≡CPh)Tp].0.5C₆H₁₄, 1·0.5C₆H₁₄. To a stirred solution of [Mo(CO)₂(η-PhC≡CPh)Tp][PF₆].CH₂Cl₂ (0.80 g, 0.933 mmol) in CH₂Cl₂ (40 cm³) was added [Co(η-C₅H₅)₂] (0.176 g, 0.933 mmol). The solution rapidly became dark green and after 10 min the solvent was removed *in vacuo*. The black residue was extracted into hot *n*-hexane (50 °C; 1 × 70 cm³, 2 × 25 cm³) and filtered through Celite. Cooling the extract to -20 °C for 18 h gave the green-black crystalline product as a 0.5 *n*-hexane solvate, yield 0.32 g (48%) (Found C, 61.0; H, 5.8; N, 12.8. C₃₄H₃₉N₆BO₂Mo requires C, 60.9; H, 5.9; N, 12.5%).

[Mo(CO)(NCMe)(η -MeC \equiv CMe)Tp][PF₆] \cdot thf, 8⁺[PF₆]⁻ \cdot thf. On stirring [Mo(CO)₂(η -MeC \equiv CMe)Tp][PF₆] (400 mg, 0.62 mmol) in MeCN (30 cm³) CO gas was evolved and the solution rapidly changed colour from yellow-green to pale blue. After 5 min the solvent was removed *in vacuo*. The blue residue was then redissolved in thf and *n*-hexane was added. On cooling the mixture to -20 °C for 6 h a pale green solid was isolated as a 1 : 1 thf solvate, yield 345 mg (76%).

[W(CO){P(OCH₂)₃CEt}(η -MeC \equiv CMe)Tp][BF₄], 10⁺[BF₄]⁻. To a stirred solution of [W(CO)₂(η -MeC \equiv CMe)Tp][BF₄] (372 mg, 0.55 mmol) in thf (30 cm³) was added P(OCH₂)₃CEt (98 mg, 0.61 mmol). The mixture was heated under reflux for 16 h and then evaporated to dryness *in vacuo*. The resulting blue solid was redissolved in CH₂Cl₂ (10 cm³), *n*-hexane (40 cm³) was added and the solution was cooled to -20 °C giving, after several days, the product as a blue, crystalline 1 : 1 CH₂Cl₂ solvate, yield 116 mg (26%).

[Mo(CO){P(OCH₂)₃CEt}(η -MeC \equiv CMe)Tp][PF₆] \cdot 0.5CH₂Cl₂, 11⁺[PF₆]⁻ \cdot 0.5CH₂Cl₂. The salt [Mo(CO)₂(η -MeC \equiv CMe)Tp][PF₆] (318 mg, 0.49 mmol) was dissolved in MeCN (40 cm³) and P(OCH₂)₃CEt (90 mg, 0.55 mmol) added. The mixture was heated under reflux for 10 min and then evaporated to dryness *in vacuo*. The green solid was redissolved in CH₂Cl₂ (10 cm³), *n*-hexane (40 cm³) was added and the volume reduced *in vacuo*, inducing precipitation of a green solid. The solid was purified by allowing *n*-hexane (50 cm³) to diffuse into a concentrated solution of the complex in CH₂Cl₂ (4 cm³) at -20 °C. This gave the product as a green, crystalline 0.5 CH₂Cl₂ solvate, yield 200 mg (47%).

The generation of [M(CO)₂(η -RC \equiv CR')Tp] (M = Mo; R = R' = Me, C₆H₄OMe-4, R = Ph, R' = H; M = W; R = R' = Me, R = Ph, R' = H) and [M(CO){P(OCH₂)₃CEt}(η -MeC \equiv CMe)Tp] (M = Mo or W) for ESR spectroscopy

To a stirred suspension of [Mo(CO)₂(η -MeC \equiv CMe)Tp][PF₆] (10.0 mg, 0.015 mmol) in toluene (2.0 cm³) was added [Co(η -C₅H₅)₂] (2.0 mg, 0.011 mmol). After 5 min the solution of [Mo(CO)₂(η -MeC \equiv CMe)Tp] was filtered and *ca.* 0.5 cm³ was transferred to a deoxygenated ESR tube. The solution was further deoxygenated by the freeze-pump-thaw method and transferred to the cavity of the ESR spectrometer. The paramagnetic complexes [Mo(CO)₂(η -RC \equiv CR')Tp] (R = R' = C₆H₄OMe-4; R = Ph, R' = H) and [W(CO)₂(η -RC \equiv CR')Tp] (R = R' = Me; R = Ph, R' = H) were generated similarly. A solution of [W(CO)₂(η -PhC \equiv CPh)Tp] (**5**) was prepared by reducing [W(CO)₂(η -PhC \equiv CPh)Tp][BF₄] with [Co(η -C₅H₅)₂] in CH₂Cl₂, evaporating the resulting mixture to dryness and then extracting the product into toluene.

Samples of [M(CO){P(OCH₂)₃CEt}(η -MeC \equiv CMe)Tp] (M = W, **10** or Mo, **11**) were prepared by adding the solid reducing agent ([Co(η -C₅Me₅)₂] and [Co(η -C₅H₅)₂] respectively) to a frozen solution of 10⁺[BF₄]⁻ or 11⁺[PF₆]⁻ in CH₂Cl₂ : thf (1 : 2) in an ESR tube. The tube was transferred to the ESR spectrometer at low temperature, and then the contents allowed to melt in order for reduction to occur. Once reaction had occurred, at the lowest temperature possible, the sample was refrozen and the anisotropic spectrum recorded. The temperature of the sample was then slowly increased until an isotropic spectrum was obtained.

Structure determinations of

[Mo(CO)₂(η -PhC \equiv CPh)Tp] \cdot 0.5C₆H₁₄, 1 \cdot 0.5C₆H₁₄, [Mo(CO)₂(η -PhC \equiv CPh)Tp][PF₆], 1⁺[PF₆]⁻ and [W(CO){P(OCH₂)₃CEt}(η -MeC \equiv CMe)Tp][BF₄] \cdot 2CH₂Cl₂, 10⁺[BF₄]⁻ \cdot 2CH₂Cl₂

Black crystals of 1 \cdot 0.5 C₆H₁₄, red-black crystals of 1⁺[PF₆]⁻ and blue crystals of 10⁺[BF₄]⁻ \cdot 2CH₂Cl₂ were grown by allowing *n*-hexane to diffuse into a solution of the complex in dichloromethane.

Crystal data for 10⁺[BF₄]⁻ \cdot 2CH₂Cl₂. C₂₈H₄₀N₆O₄B₂Cl₄F₄PW: *M* = 978.90, monoclinic, space group *P*2₁/*c*, *a* = 15.065(2), *b* = 21.148(4), *c* = 13.192(2) Å, β = 114.27(2)°, *V* = 3831.5(9) Å³, *T* = 173 K, *Z* = 4, μ = 3.397 mm⁻¹, reflections collected = 24687, independent reflections (*R*_{int}) = 8790 (0.0393), final *R* indices [*I* > 2 σ (*I*): *R*₁, *wR*₂ = 0.0292, 0.0646. Crystal data for 1 \cdot 0.5 C₆H₁₄ and 1⁺[PF₆]⁻ are given in ref. 3; CCDC reference codes are RAPCOA and RAPCOG respectively.

CCDC reference number 287241.

For crystallographic data in CIF or other electronic format see DOI: 10.1039/b514951g

Acknowledgements

We thank the EPSRC (D.J.H. and O.D.H.), the University of Bristol (I.M.B. and M.J.Q.) and the Royal Thai Government (S.B.) for Postgraduate Scholarships. We also thank Dr Zbigniew Sojka (Jagiellonian University, Krakow) for simulating the ESR spectrum of complex **11** using genetic algorithm methods.

References and notes

- N. G. Connelly, W. E. Geiger, M. C. Lagunas, B. Metz, A. L. Rieger, P. H. Rieger and M. J. Shaw, *J. Am. Chem. Soc.*, 1995, **117**, 12202; N. G. Connelly, B. Metz, A. G. Orpen and P. H. Rieger, *Organometallics*, 1996, **15**, 729; N. G. Connelly, W. E. Geiger, S. R. Lovelace, B. Metz, T. J. Paget and R. Winter, *Organometallics*, 1999, **18**, 3201; I. M. Bartlett, N. G. Connelly, A. J. Martin, A. G. Orpen, T. J. Paget, A. L. Rieger and P. H. Rieger, *J. Chem. Soc., Dalton Trans.*, 1999, 691; I. M. Bartlett, S. Carlton, N. G. Connelly, D. J. Harding, O. D. Hayward, A. G. Orpen, C. D. Ray and P. H. Rieger, *Chem. Commun.*, 1999, 2403; C. J. Adams, N. G. Connelly and P. H. Rieger, *Chem. Commun.*, 2001, 2458; C. J. Adams, K. M. Anderson, N. G. Connelly, D. J. Harding, A. G. Orpen, E. Patron and P. H. Rieger, *Chem. Commun.*, 2002, 130; C. J. Adams, K. M. Anderson, I. M. Bartlett, N. G. Connelly, A. G. Orpen and T. J. Paget, *Organometallics*, 2002, **21**, 3454.
- C. J. Adams, I. M. Bartlett, N. G. Connelly, D. J. Harding, O. D. Hayward, A. J. Martin, A. G. Orpen, M. J. Quayle and P. H. Rieger, *J. Chem. Soc., Dalton Trans.*, 2002, 4281.
- I. M. Bartlett, N. G. Connelly, A. G. Orpen, M. J. Quayle and J. C. Rankin, *Chem. Commun.*, 1996, 2583.
- S. G. Feng, C. C. Philipp, A. S. Gamble, P. S. White and J. L. Templeton, *Organometallics*, 1991, **10**, 3504.
- J. L. Templeton and B. C. Ward, *J. Am. Chem. Soc.*, 1980, **102**, 3288.
- J. L. Templeton, *Adv. Organomet. Chem.*, 1989, **29**, 1.
- J. L. Templeton, J. L. Caldarelli, S. G. Feng, C. C. Philipp, M. B. Wells, B. E. Woodworth and P. S. White, *J. Organomet. Chem.*, 1994, **478**, 103.
- D. J. Harding, Ph.D. Thesis, University of Bristol, 2000.
- S. G. Feng and J. L. Templeton, *Organometallics*, 1992, **11**, 2168.
- S. R. Allen, P. K. Baker, S. G. Barnes, M. Green, L. Trollope, L. Manojlovic-Muir and K. M. Muir, *J. Chem. Soc., Dalton Trans.*, 1981, 873.
- T. Spalek, P. Pietrzyk and Z. Sojka, *Acta Phys. Pol.*, 2005, **108**, 95; T. Spalek, P. Pietrzyk and Z. Sojka, *J. Chem. Inf. Model.*, 2005, **45**, 18.
- P. H. Rieger, *Coord. Chem. Rev.*, 1994, **135-136**, 203.
- P. H. Rieger, *J. Magn. Reson.*, 1997, **124**, 140.

- 14 J. R. Morton and K. F. Preston, *J. Magn. Reson.*, 1978, **30**, 577.
- 15 *Jaguar 5.0*, Schrodinger, LLC, Portland, Oregon, 2002.
- 16 The LACV3P basis set is a triple-zeta contraction of the LACVP basis set that is peculiar to the Jaguar programme. LACVP uses an effective core potential to describe all but the valence nd , $(n + 1)s$ and $(n + 1)p$ and outer core ns and np electrons. P. J. Hay and W. R. Wadt, *J. Chem. Phys.*, 1985, **82**, 270.
- 17 E. D. Glendening, J. K. Badenhoop, A. E. Reed, J. E. Carpenter, J. A. Bohmann, C. M. Morales and F. Weinhold, *NBO 5.0*, Theoretical Chemistry Institute, University of Wisconsin, Madison, WI, 2001; <http://www.chem.wisc.edu/~nbo5>.
- 18 G. Frenking, K. Wichmann, N. Fröhlich, J. Grobe, W. Golla, D. Le Van, B. Krebs and M. Läge, *Organometallics*, 2002, **21**, 2921.
- 19 M. K. Munzarová, DFT calculations of EPR hyperfine coupling constants, in *Calculation of NMR and EPR parameters*, ed. M. Kaupp, M. Bühl and V. G. Malkin, Wiley-VCH, Weinheim, 2004, ch. 29.
- 20 K.-B. Shiu and L.-Y. Lee, *J. Organomet. Chem.*, 1988, **348**, 357.
- 21 N. G. Connelly and W. E. Geiger, *Chem. Rev.*, 1996, **96**, 904.
- 22 R. B. King, *Organometallic Syntheses*, Academic Press, New York, 1965, vol. 1, p. 70.
- 23 U. Koelle and F. Khouzami, *Chem. Ber.*, 1981, **114**, 2929.